© 2022. Published by The Company of Biologists Ltd | Development (2022) 149, dev200696. doi:10.1242/dev.200696

RESEARCH ARTICLE

Paternally inherited H3K27me3 affects chromatin accessibility in mouse embryos produced by round spermatid injection

Mizuki Sakamoto[1], Daiyu Ito[1], Rei Inoue[1], Sayaka Wakayama[2], Yasuyuki Kikuchi[1], Li Yang[1], Erika Hayashi[1], Rina Emura[1], Hirosuke Shiura[1], Takashi Kohda[1], Satoshi H. Namekawa[3], Takashi Ishiuchi[1,‡], Teruhiko Wakayama[2] and Masatoshi Ooga[1,*,‡]

ABSTRACT

Round spermatid injection (ROSI) results in a lower birth rate than intracytoplasmic sperm injection, which has hampered its clinical application. Inefficient development of ROSI embryos has been attributed to epigenetic abnormalities. However, the chromatin-based mechanism that underpins the low birth rate in ROSI remains to be determined. Here, we show that a repressive histone mark, H3K27me3, persists from mouse round spermatids into zygotes in ROSI and that round spermatid-derived H3K27me3 is associated with less accessible chromatin and impaired gene expression in ROSI embryos. These loci are initially marked by H3K27me3 but undergo histone modification remodelling in spermiogenesis, resulting in reduced H3K27me3 in normal spermatozoa. Therefore, the absence of epigenetic remodelling, presumably mediated by histone turnover during spermiogenesis, leads to dysregulation of chromatin accessibility and transcription in ROSI embryos. Thus, our results unveil a molecular logic, in which chromatin states in round spermatids impinge on chromatin accessibility and transcription in ROSI embryos, highlighting the importance of epigenetic remodelling during spermiogenesis in successful reproduction.

KEY WORDS: Zygotic genome activation, Chromatin remodelling, Round spermatid injection, H3K27me3, Epigenetic inheritance, Spermiogenesis

INTRODUCTION

Round spermatid injection (ROSI) is a valuable and the sole method for obtaining offspring from patients with male infertility due to spermatogenesis disruption, especially nonobstructive azoospermia (NOA) (Tekayev and Vuruskan, 2021; Tesarik et al., 1996). Embryos produced by ROSI (ROSI embryos) can develop to term in mice, rabbits, rats and humans (Hirabayashi et al., 2002; Kimura and Yanagimachi, 1995b; Ogura et al., 1994; Sofikitis et al., 1994; Tesarik et al., 1995). Nevertheless, the success rate of full-term development following ROSI is lower than intracytoplasmic sperm injection (ICSI) embryos. Furthermore, despite reports that healthy offspring were obtained using ROSI in humans, the therapeutic application of ROSI has not been widely adopted due to its uncertain safety (Aslam et al., 1998; Tanaka et al., 2015, 2018; Tekayev and Vuruskan, 2021). Therefore, toward its clinical application, it is important to understand at the molecular level why ROSI embryos show poor development. Current research implies transmitted histone proteins from round spermatid cause abnormalities in the epigenome, transcriptome and, consequently, embryonic development of ROSI embryos (Hayashi et al., 2003; Kishigami et al., 2006). Ectopic accumulation of a repressive mark H3K9me3 has been found in male pronuclei (PN) in one-cell ROSI embryos at the pericentromeric heterochromatin regions, suggesting the presence of histone marks inherited from round spermatids (Kishigami et al., 2006). However, the role of paternal chromatin and molecular underpinning of the abnormal transcriptome and poor embryonic development in ROSI embryos remains to be elucidated.

Male germ cells that reached the haploid round spermatid stage undergo dynamic morphological and physiological changes to form sperm capable of fertilization. This process is known as spermiogenesis and the chromatin structure changes dynamically: histones are replaced by protamine in order to pack the genome into a highly condensed state in sperm (Rathke et al., 2014). Thereby, histone content in sperm is dramatically reduced during spermiogenesis and, accordingly, the distribution of histone modifications and variants, which are tightly linked to gene expression, is dynamically altered (Erkek et al., 2013; Tatehana et al., 2020). Despite the global reduction in histone levels, histones in certain genomic regions are retained in sperm and are considered to be inherited into zygotes (Erkek et al., 2013; Hammoud et al., 2009; Jung et al., 2019; Yamaguchi et al., 2018; Yoshida et al., 2018). Furthermore, perturbation of an active histone methylation mark (H3K4me3) during spermatogenesis disturbs embryonic development (Lismer et al., 2020; Siklenka et al., 2015), highlighting the importance of inherited epigenome information for embryonic gene expression. In addition to H3K4me3, H3K27me3, a polycomb repressive complex 2 (PRC2)-mediated repressive mark, is also considered an inheritable epigenetic mark that regulates embryonic gene expression, and H3K4me3 and H3K27me3 together form a bivalent chromatin domain that represents germline developmental potential (Erkek et al., 2013; Lesch et al., 2013, 2016; Maezawa et al., 2018b; Sin et al., 2015; Teperek et al., 2016). Therefore, the fact that ROSI embryos receive more histones than ICSI embryos is likely to be linked to the presence of excessive and undesired histone marks, which may adversely influence the chromatin accessibility landscape and embryonic transcriptome.

We hypothesised that epigenetic information in round spermatids may be transferred to ROSI embryos, leading to detrimental effects

[1]Faculty of Life and Environmental Sciences, University of Yamanashi, Yamanashi, 400-8510, Japan. [2]Advanced Biotechnology Center, University of Yamanashi, Yamanashi, 400-8510, Japan. [3]Department of Microbiology and Molecular Genetics, University of California Davis, Davis, CA 95616, USA.
*Present address: Department of Animal Science and Biotechnology, School of Veterinary Medicine, Azabu University, Kanagawa, 252-5201, Japan.

‡Authors for correspondence (tishiuchi@yamanashi.ac.jp; ohga@azabu-u.ac.jp)

H.S., 0000-0003-2553-6971; S.H.N., 0000-0002-1052-943X; T.I., 0000-0001-8346-4596; T.W., 0000-0002-6151-2603; M.O., 0000-0002-0721-7750

Handling Editor: Haruhiko Koseki
Received 26 February 2022; Accepted 14 August 2022

Development (2022) 149, dev200696. doi:10.1242/dev.200696

in the regulation of gene expression or chromatin remodelling processes that are important for embryonic development. Therefore, in this study, we performed a comparative analysis between mouse embryos generated either by ROSI or ICSI using transposase-accessible chromatin sequencing (ATAC-seq) and RNA-seq. We identified differences in chromatin accessibility as well as gene expression, which were potentially triggered by carried-over epigenetic information. Notably, we found that chromatin regions marked by H3K27me3 in round spermatids, but not in mature sperm, are associated with lower accessibility and influence gene expression at zygotic genome activation (ZGA). Therefore, our results demonstrate that spermiogenesis completion is crucial for establishing a normal chromatin accessibility landscape as well as for proper embryonic gene expression.

RESULTS

The chromatin accessibility landscape and transcriptome in ROSI and ICSI embryos

To investigate the differences in chromatin accessibility and transcriptome between ROSI and ICSI embryos, we performed an assay using ATAC-seq and RNA-seq for ROSI and ICSI embryos at the one- and two-cell stages (Fig. 1A). We selected embryos with two PN with normal morphology and one-cell samples were used after 12-13 h post-activation (hpa) or injection (hpi) (for ROSI or ICSI, respectively) and 28-30 h for two-cell samples. In the ATAC-seq, as the number of available embryos upon ROSI and ICSI was limited, we employed Omni ATAC-seq, an improved ATAC-seq protocol (Gou et al., 2020; Corces et al., 2017). We used 400-450 zygotes and blastomeres per sample with the removal of the first and second polar bodies (PB) (Fig. 1B). We prepared two biological replicates and obtained at least 21 million reads uniquely mapped to the genome per sample. We also performed RNA-seq. We confirmed that reproducible data were obtained from biological replicates and that our ATAC-seq data for ICSI two-cell embryos showed high similarity with published ATAC-seq data for two-cell embryos (Wu et al., 2016) (Fig. 1C; Fig. S1A-E). Importantly, in contrast to a previous report in which ATAC-seq peaks (ATAC peaks) were undetectable at the one-cell stage (Wu et al., 2016), we detected clear ATAC signals using an improved method.

We first found that ATAC-seq signals in ROSI and ICSI embryos show globally similar profiles, suggesting that chromatin remodelling normally occurs in ROSI embryos (Fig. 1C,D). As expected, ATAC peaks that represent open chromatin regions (Table S1), were observed at active chromatin regions enriched in H3.3 and H3K4me3, but not at H3K27me3-marked repressive chromatin regions in ICSI or ROSI two-cell embryos (Ishiuchi et al., 2021; Liu et al., 2016; Wang et al., 2018; Wu et al., 2016) (Fig. 1C,D). H3K9me3 was enriched at the transcription start sites (TSSs) associated with relatively high accessibility at the two-cell stage. This may reflect a non-repressive function of H3K9me3 at these embryonic stages (Burton et al., 2020; Wang et al., 2018). Similar tendencies were also observed in ICSI or ROSI one-cell embryos, but under a weaker correlation with active marks. This is expected, as H3.3 and H3K4me3 show non-canonical distribution at the one-cell stage (Ishiuchi et al., 2021; Zhang et al., 2016). For a more detailed analysis of open chromatin regions, we classified gene promoter regions into four clusters by *k*-means clustering based on the strength of ATAC peaks of one-cell ROSI, one-cell ICSI, two-cell ROSI and two-cell ICSI embryos. Promoter ATAC signals were positively correlated with gene expression levels. Given the inheritance of maternal mRNA into one-cell embryos, the positive correlation between gene expression and ATAC-seq signals at the one-cell stage may indicate that genes actively transcribed in oocytes have high promoter accessibility, even at the one-cell stage (Fig. 1D). Notably, in clusters 1, 2 and 3, we observed gene expression upregulation during development to the two-cell stage (Fig. S1F), although ATAC signals at their promoters diminished (Fig. 1D). These findings suggest that promoter accessibility correlates with transcriptional output; however, is not the determinant. Therefore, other factors than promoter accessibility may cooperatively fine-tune transcriptional output during ZGA.

Identifying differentially expressed genes in ROSI embryos

We next investigated how transcriptome is affected in ROSI embryos. We identified 186 upregulated and 16 downregulated genes in ROSI embryos at the one-cell stage [termed as one-cell ROSI-high and one-cell ROSI-low differentially expressed genes (DEGs), respectively] [false discovery rate (FDR)<0.01, fold change (FC)>1.5], and 649 upregulated and 513 downregulated genes were detected at the two-cell stage (Fig. 2A,B). At the one-cell stage, most DEGs were upregulated genes and their gene expression in ICSI embryos was extremely limited (Fig. 2A; Fig. S2A). As the transcription activity at the one-cell stage is low, we considered that a higher abundance of these transcripts in ROSI one-cell embryos may reflect carry-over of RNA from round spermatids. To test this hypothesis, we first performed gene ontology (GO) analysis of these genes and identified the terms ‘sperm motility’ and ‘spermatogenesis’ (Fig. 2C). Indeed, transition proteins *Tp1* (also known as *Tnp1*) and *Tp2* (*Tnp2*), which play a crucial role in spermiogenesis during histone-protamine replacement (Zhao et al., 2004), were contained, which is consistent with a previous study (Hayashi et al., 2003). We then analyzed published RNA-seq data for cells at different spermatogenesis stages to examine their gene expression levels (Hasegawa et al., 2015; Kobayashi et al., 2012). The expression levels of these genes peaked at the round spermatid stage and decreased during maturation into sperm (Fig. 2D). To further investigate this observation, we performed qRT-PCR. For this assay, we prepared one-cell ROSI embryos treated with or without 5,6-dichloro-1-β-D-ribofuranosyl-benzimidazole (DRB), which blocks zygotic transcription. Transcripts of one-cell ROSI-high DEG genes, *Tp1*, *Tp2* and *Smcp* showed much higher abundance in ROSI embryos than ICSI embryos, and their higher abundance was not affected by DRB treatment (Fig. 2E). In contrast, zygotically expressed genes, such as *Klf5*, were significantly decreased by DRB treatment (Fig. S2B). These results strongly indicate that round spermatid-derived RNA is transferred into ROSI one-cell embryos.

At the two-cell stage, when embryos undergo major ZGA, DEGs were identified in ROSI embryos (Fig. 2B). We again performed GO analysis and found spermatogenesis-related genes were still enriched in the upregulated gene group in ROSI two-cell embryos (two-cell ROSI-high DEGs) (Fig. 2C). Accordingly, 54 genes of the two-cell ROSI-high DEGs overlapped with the one-cell ROSI-high DEGs (Fig. S2C) and the upregulated status of these 54 genes were maintained between ROSI one-cell and two-cell embryos (Fig. S2D). Therefore, RNA carry-over from round spermatids appears to still contribute to differential gene expression at the two-cell stage. However, its contribution to overall differential expression is small, suggesting ZGA may be affected in ROSI two-cell embryos. To gain further insight into the mechanisms underlying differential gene expression in ROSI two-cell embryos, we analyzed promoter chromatin accessibility. However, there were

Development (2022) 149, dev200696. doi:10.1242/dev.200696

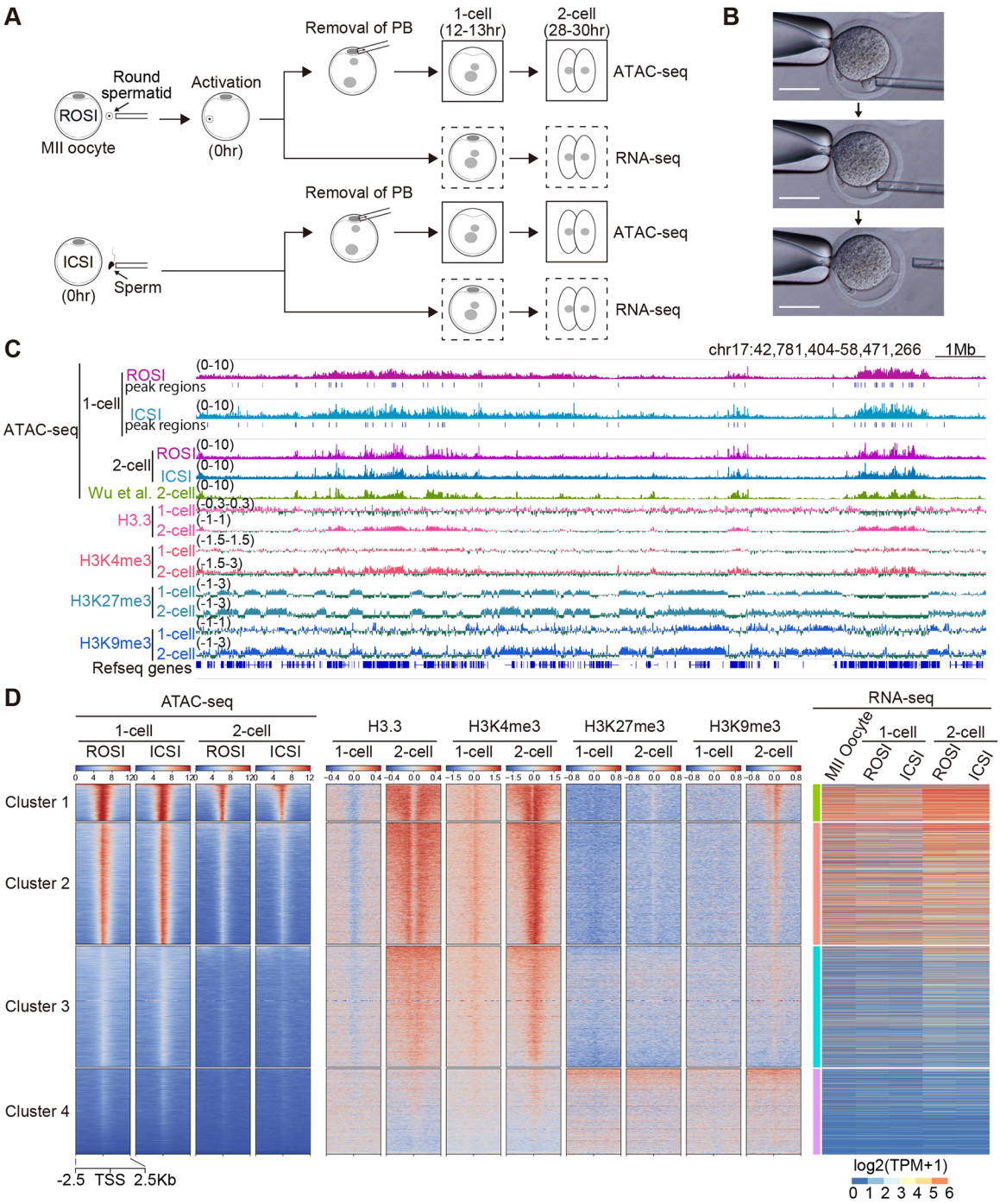

Fig. 1. Chromatin accessibility landscape in ROSI embryos. (A) Schematic showing the sample preparation process for chromatin accessibility and transcriptome analyses in ROSI and ICSI embryos. The collected samples for ATAC-seq and RNA-seq are indicated by solid and dotted boxes, respectively. PB, polar body. (B) Images showing the process of polar body removal for ATAC-seq. Scale bars: 50 µm. (C) Genome browser snapshots showing ATAC-seq data and ChIP-seq data for indicated histone modifications or H3.3. ATAC-seq data for two-cell embryos and ChIP-seq data for H3.3, H3K4me3, H3K27me3 and H3K9me3 for one-cell and two-cell data from GSE66390, GSE139527, GSE97778 and GSE73952, respectively (Ishiuchi et al., 2021; Liu et al., 2016; Wang et al., 2018; Wu et al., 2016). ATAC-seq data are shown as reads per kilobase per million reads (RPKM) and ChIP-seq data are shown as log2 ratios between ChIP and input samples. (D) Left, heatmaps showing normalized ATAC-seq, H3.3, H3K4me3, H3K27me3 and H3K9me3 around transcription start site (TSS) regions. The ATAC signal patterns of one-cell ROSI, one-cell ICSI, two-cell ROSI and two-cell ICSI were subjected to *k*-means clustering and showed clusters 1-4. Right, expression levels of corresponding genes in MII oocyte (E-MTAB-2950; Abe et al., 2015), ROSI and ICSI embryos. Transcriptional levels are indicated by transcripts per million (TPM) (see also Fig. S1F).

no obvious differences in chromatin accessibility at the promoters of DEGs between ICSI and ROSI embryos (Fig. 2F), suggesting chromatin accessibility at their promoter is not globally related to the altered transcriptome of ROSI embryos.

Identifying chromatin regions with differential accessibility in ROSI embryos

Although ATAC-seq signals were not altered at the DEG promoter regions, we speculated that differential chromatin accessibility

Development (2022) 149, dev200696. doi:10.1242/dev.200696

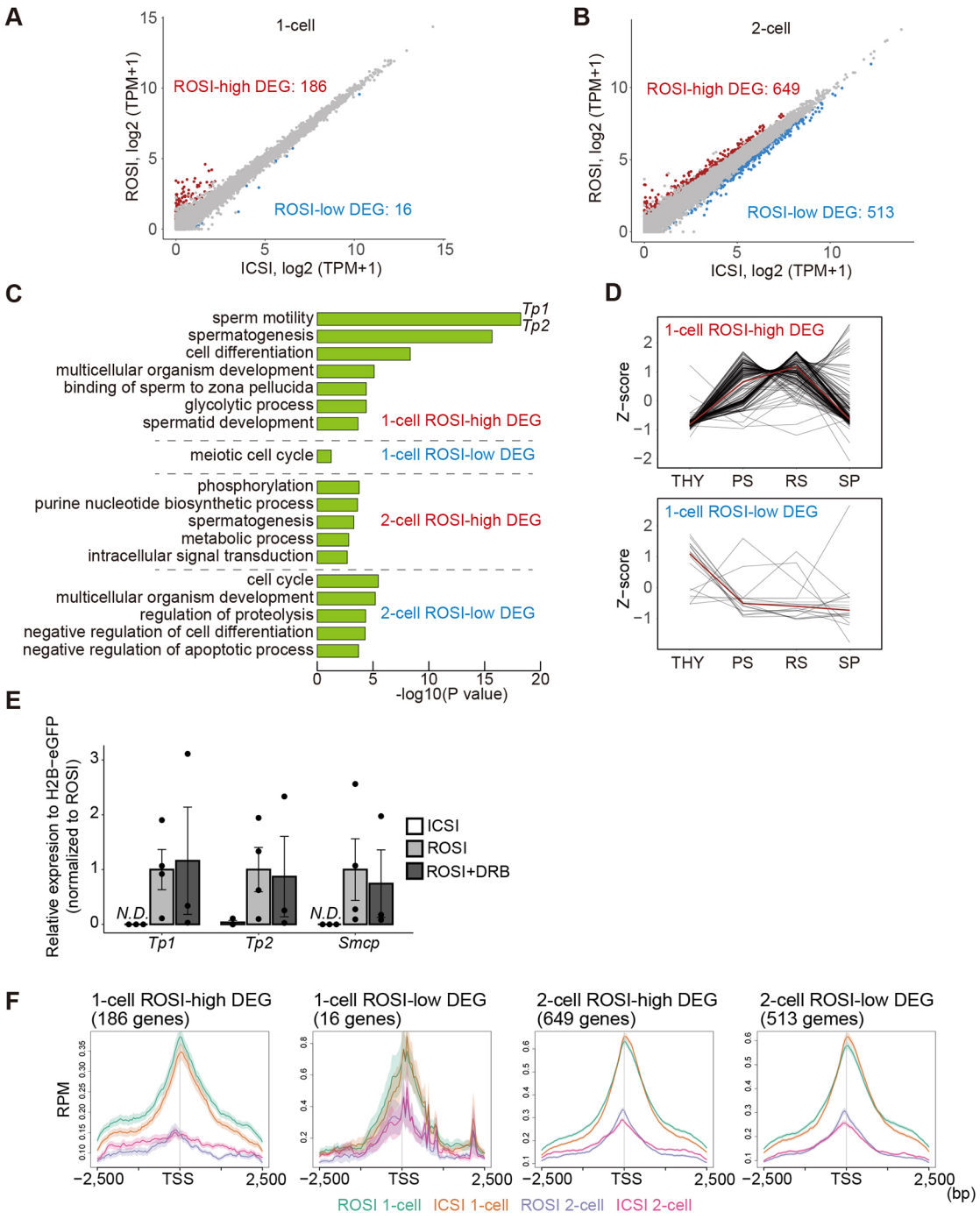

Fig. 2. Differentially expressed genes (DEGs) in ROSI embryos. (A,B) Scatter plots comparing gene expression levels between ROSI and ICSI embryos at the one-cell stage (A) or two-cell stage (B). Upregulated genes (FDR<0.01 and FC>1.5, indicated as ROSI-high) and downregulated genes (FDR<0.01 and FC>1.5, indicated as ROSI-low) in ROSI embryos are coloured with red and blue, respectively. (C) Gene ontology (GO) analysis of the four DEG groups indicated in A and B. *Tp1* and *Tp2* were included in the term 'sperm motility'. (D) Gene expression kinetics of one-cell DEGs during spermatogenesis. Published RNA-seq data (GSE55060 and DRA000484) (Hasegawa et al., 2015; Kobayashi et al., 2012) were used and shown as *z*-scores based on TPM values. THY, undifferentiated spermatogonia; PS, pachytene spermatocytes; RS, round spermatid; SP, sperm. (E) Quantitative real-time polymerase chain reaction (qRT-PCR) confirmation of RNA transmission from round spermatid. DRB inhibits transcription as reported by Abe et al., 2018 (see also Fig. S2A). qRT-PCR analyses of one-cell ROSI-high genes (*Tp1*, *Tp2* and *Smcp*) in ICSI, ROSI and DRB-treated ROSI one-cell embryos (at least three biological replicates). Gene expression was first normalized using the expression of H2B-eGFP as external control and divided by the mean value of ROSI embryos. Data are mean±s.e.m. Dots indicate each data point. Values not detected (N.D.) were represented as 0. (F) Chromatin accessibility at promoters of each DEG group. Accessibilities of ROSI one-cell, ICSI one-cell, ROSI two-cell, and ICSI two-cell are coloured differently. ATAC-seq data are shown as RPM (read count per million mapped reads).

outside of these promoters may be associated with abnormal development of ROSI embryos. We then first performed quantitative analysis of ATAC-seq data (see Materials and Methods) and identified ATAC peaks showing higher or lower accessibility in ROSI embryos compared with ICSI embryos (referred to as ROSI-high and ROSI-low ATAC peaks, respectively). Although the number of these peaks was limited and more than 90% of total ATAC peaks remained unchanged

Development (2022) 149, dev200696. doi:10.1242/dev.200696

between ICSI and ROSI embryos (classified as common peaks) (Fig. 3A), we further investigated the potential cause of differential chromatin accessibility. The number of ROSI-high peaks was consistently higher than ROSI-low peaks in one- and two-cell ROSI embryos, and ROSI-high peaks at the one-cell stage were frequently observed within the intronic or intergenic region (Fig. 3B; Fig. S3A). Only a few cases of ROSI-high or -low peaks were commonly detected between one- and two-cell stages (Fig. S3B). Therefore, most of these differential peaks were developmental stage-specific. Because altered chromatin accessibility upon ROSI application is highly represented in one-cell ROSI embryos, we decided to focus on differential chromatin accessibility at the one-cell stage for further analysis.

To characterize one-cell ROSI-high and -low ATAC peaks, we analyzed published chromatin immunoprecipitation sequencing (ChIP-seq) data for epigenetic marks in normal embryos (H3.3,

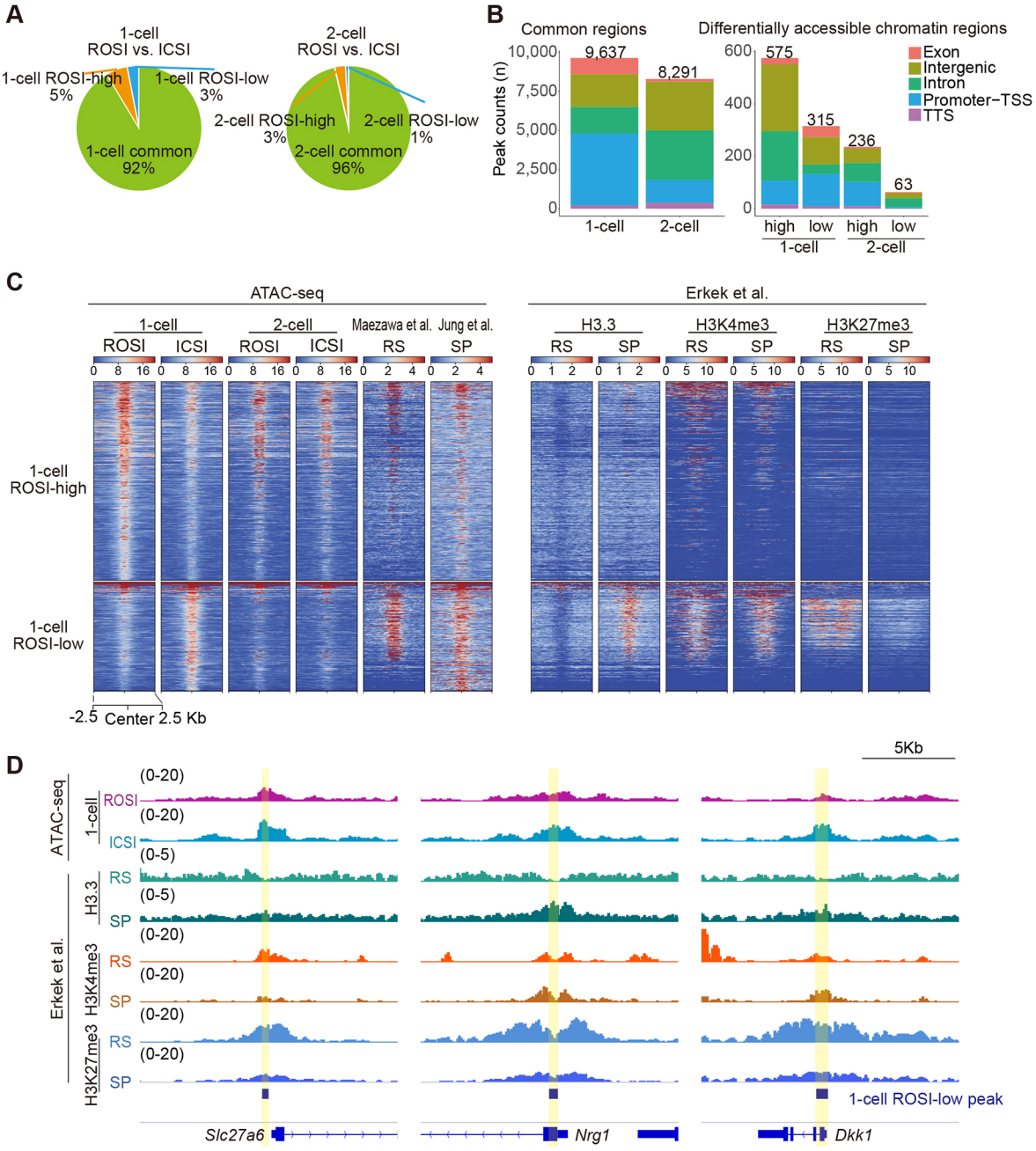

Fig. 3. Differentially accessible chromatin regions in ROSI embryos indicate signs of epigenetic inheritance from round spermatids. (A) The fraction of ATAC peaks is classified into common, ROSI-high or ROSI-low at the one-cell stage (left) or two-cell stage (right). Differentially accessible chromatin regions were detected using MACS and MAnorm (see Materials and Methods). (B) The genomic location of each peak. TSS, transcription start site; TTS, transcription termination site. (C) Heatmaps showing ATAC-seq data (left) and ChIP-seq data for H3.3, H3K4me3 and H3K27me3 in differentially accessible chromatin regions. ATAC-seq and ChIP-seq data for round spermatid (RS) and sperm (SP) were obtained from GSE102954, GSE116857 and GSE42629 (Erkek et al., 2013; Jung et al., 2019; Maezawa et al., 2018a). Heatmaps are shown with RPKM. See also Fig. S4A,B. (D) Genome browser snapshots showing representative genomic regions with decreased promoter chromatin accessibility in one-cell ROSI embryos. One-cell ROSI-low peak regions are highlighted in light yellow. See also Fig. S5.

Development (2022) 149, dev200696. doi:10.1242/dev.200696

H3K4me3, H3K27me3 and H3K9me3) (Ishiuchi et al., 2021; Liu et al., 2016; Wang et al., 2018). One-cell ROSI-high ATAC peak regions were characterized by weak enrichment of H3K4me3, suggesting that accessible regions are excessively formed in regions where H3K4me3 is not normally enriched (Fig. S3C,D). On the other hand, one-cell ROSI-low ATAC peak regions were the regions in which H3K4me3 but not H3K27me3 is normally enriched. These features were similarly observed at randomly selected ATAC peak regions. Thus, this indicates that one-cell ROSI-low peak regions display a general feature of accessible regions in normal one-cell embryos and that accessibility of a small fraction of these H3K4me3-marked and H3K27me3-depleted regions become lower in one-cell ROSI embryos. Moreover, enrichment of H3K4me3 at these regions tended to be maintained during early development as well as in embryonic stem cells (ESCs), while H3K27me3 was not enriched (Fig. S3E). Therefore, these results indicate that chromatin accessibility decreased at generally active chromatin regions in one-cell ROSI embryos. We then speculated that undesirable inheritance of epigenetic information from round spermatids to ROSI embryos may result in differential chromatin accessibility. To explore this possibility, we analyzed published ATAC-seq and ChIP-seq data for round spermatids and sperm (Erkek et al., 2013; Jung et al., 2019; Maezawa et al., 2018a) (Fig. 3C). We observed higher chromatin accessibility in sperm compared with round spermatids irrespective of one-cell ROSI-high or one-cell ROSI-low ATAC peak regions (Fig. 3C; Fig. S4A,B). Thus, the differences in chromatin accessibility between round spermatids and sperm did not correlate with differential chromatin accessibility between one-cell ROSI and ICSI embryos. Histone H3.3, enrichment of which around the CpG-rich promoters in sperm reflects histone retention (Erkek et al., 2013), was enriched at the one-cell ROSI-low ATAC peak regions, but not at the one-cell ROSI-high ATAC peak regions in sperm, suggesting one-cell ROSI-low ATAC peak regions are the regions in which histones are preferentially retained (Fig. 3C). Interestingly, although H3K4me3 enrichment at one-cell ROSI-high or ROSI-low peak regions was similar between round spermatids and sperm, we observed higher H3K27me3 enrichment in round spermatids compared with sperm at the one-cell ROSI-low peak regions (Fig. 3C,D; Fig. S4A,B). This observation was confirmed by analyzing other publicly available datasets (Hammoud et al., 2014; Iwamori et al., 2016; Jung et al., 2017) (Fig. S4C). This indicates that H3K27me3-enriched chromatin regions in round spermatids, in which its enrichment becomes weaker during maturation into sperm, show lower chromatin accessibility in one-cell ROSI embryos. Notably, this lower chromatin accessibility was cancelled at the two-cell stage (Fig. 3C; Fig. S3B), thus these changes in accessibility appear to be transient. To explore our hypothesis that H3K27me3 in round spermatids affects the chromatin accessibility in ROSI embryos, we analyzed the enrichment of H3K27me3 and H3K4me3 at the one-cell ROSI-high and -low ATAC peak regions as well as at the randomly selected regions in round spermatids. Importantly, we observed significant enrichment of H3K27me3 at the one-cell ROSI-low ATAC peak regions (Fig. S4D,E). In addition, this region was also mildly enriched in H3K4me3 (Fig. S4D,E). Altogether, these data suggest that chromatin accessibility at regions generally marked by active H3K4me3 in early embryos is suppressed in one-cell ROSI embryos, possibly due to the inheritance of H3K27me3-marked repressive chromatin states from round spermatids.

To further test our hypothesis that repressive chromatin status is inherited from round spermatids, we performed immunostaining for H3K27me3 at the one- and two-cell stages. To distinguish paternal and maternal chromatin, we also performed immunostaining for H3K9me2, stronger signals of which were observed on the maternal chromatin at the one- and two-cell stages (Burton and Torres-Padilla, 2010). Similar to the previous observation for H3K9me3 (Kishigami et al., 2006), ectopic H3K9me2 signals were observed at the pericentromeric heterochromatin region in male PN of ROSI one-cell embryos (Fig. 4A,B). On the contrary, at the one-cell stage, H3K27me3 intensity in male PN in ROSI embryos was globally higher than that in ICSI embryos (Fig. 4A,B). Furthermore, consistent with this observation, asymmetric H3K27me3 signals between parental chromosomes in ICSI two-cell embryos was not observed in ROSI two-cell embryos (Fig. 4C). Round spermatids showed higher signals for H3K27me3, but not sperm (Fig. 4D), suggesting ROSI embryos may possess an abnormal landscape of H3K27me3 by inheriting this mark from round spermatids. We also asked whether there are any other histone marks that would alter chromatin accessibility in ROSI embryos. Among the histone marks analyzed (H3K4me1, H3K4me3, H3K27me3 and H3K36me3), remodelling of H3K4me1 during spermiogenesis was also observed, but this modification was similarly enriched in both one-cell ROSI-high and low ATAC peak regions (Fig. S4C). Thus, at this point, H3K27me3 is the only histone mark tightly associated with altered chromatin accessibility in ROSI embryos.

Altered chromatin accessibility in ROSI embryos affects transcription

H3K27me3 represses gene expression (reviewed by Zhang et al., 2015). Therefore, we next investigated whether lower chromatin accessibility in ROSI one-cell embryos is associated with changes in gene expression. We classified ATAC peaks into distal ATAC peaks and promoter ATAC peaks (peaks at TSS±1 kb). We observed no changes in gene expression when focused on distal ATAC peaks or ROSI-high ATAC peaks (Fig. 5A). In contrast, gene expression associated with ROSI-low promoter ATAC peaks (146 genes) was lower than ICSI embryos (Fig. 5A; Fig. S5A-D). Lower expression was prominent at the two-cell stage, which suggests that promoter chromatin accessibility at the one-cell stage might be important for future gene activation. Furthermore, we found that the one-cell ROSI-low promoter ATAC peaks that show H3K27me3 enrichment in round spermatids (H3K27me3 RPKM>1 in round spermatid) are mainly associated with this lower gene expression (Fig. S6A). Notably, although the tendency of downregulation was observed in this gene group, only a few DEGs (FDR<0.01 and FC>1.5, as seen in Fig. 2B) were included (Fig. 5B), indicating that lower chromatin accessibility only mildly affects transcription.

Our immunostaining data revealed that the distribution of H3K27me3 in ROSI embryos differed largely from ICSI embryos, and therefore we hypothesised that inheritance of H3K27me3 from round spermatids may suppress gene expression without altering chromatin accessibility. We then analyzed H3K27me3 and H3K4me3 enrichment in round spermatids or sperm around the TSSs of DEGs at the two-cell stage. Interestingly, prominent enrichment of H3K27me3 as well as mild enrichment of H3K4me3 was observed at the ROSI-low DEG promoters in round spermatids, but H3K27me3 enrichment diminished in sperm (Fig. 5C,D; Fig. S6B). In contrast, weaker H3K27me3 enrichment as well as higher enrichment of H3K4me3 was observed at the ROSI-high DEG promoters in round spermatids, indicating that the promoters of two-cell high and low DEGs possess bivalent H3K4me3 and H3K27me3 modifications at different levels in round spermatids. Given the previous observation that bivalent promoters in round spermatids are prevalent for genes expressed

Development (2022) 149, dev200696. doi:10.1242/dev.200696

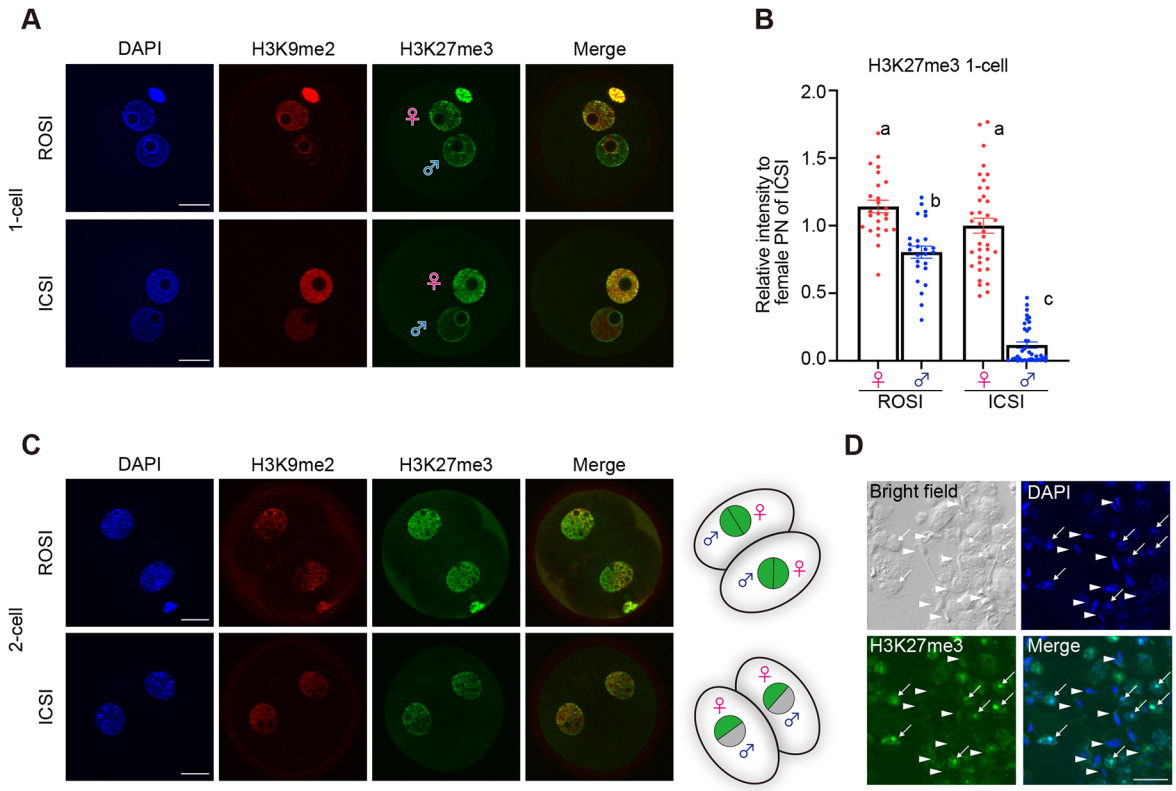

Fig. 4. Immunostaining for H3K27me3 in ROSI and ICSI embryos. (A) Images of immunostaining for H3K27me3 and H3K9me2 in ROSI and ICSI embryos at the one-cell stage. (B) Plots showing H3K27me3 signal intensity in the female and male pronuclei (PN) of one-cell embryos. Values are normalized by the signal intensity of DAPI. Different characters indicate significant differences (P<0.05, one-way ANOVA and Tukey's multi-comparisons test). Data are mean±s.e.m. n=37 (ROSI embryos) and n=25 (ICSI embryos). (C) Images of immunostaining for H3K27me3 and H3K9me2 in ROSI and ICSI embryos at the two-cell stage. n=31 (ROSI embryos) and n=28 (ICSI embryos). Schematic shows that both parental regions have H3K27me3 in ROSI embryos but not in ICSI embryos at the two-cell stage. (D) Images of immunostaining for H3K27me3 in spermatogenic cells. Minced seminiferous tubules were subjected to immunostaining. Sperm (SP) and round spermatid (RSs) are shown as arrowheads and arrows, respectively. Scale bars: 20 µm.

after fertilization (Lesch et al., 2013, 2016; Maezawa et al., 2018b; Sin et al., 2015), our results suggest that removal of H3K27me3 during spermiogenesis might be prerequisite for proper embryonic transcription.

Identification of transcription factor motifs at the chromatin regions with differential accessibility

The results above indicated that the inheritance of repressive chromatin status from round spermatids might cause lower chromatin accessibility and altered gene expression in ROSI embryos. However, we did not find any possible involvement of histone modifications in acquisition of higher chromatin accessibility in ROSI embryos (Fig. 3C; Fig. S4C). Thereby, we suspected that an alternative mechanism such as a transcription factor (TF)-driven mechanism might be involved in this process. To explore this possibility, we performed a TF motif analysis on one-cell ROSI-high, ROSI-low and ROSI-common ATAC peaks. We obtained some TF motifs at these peaks (Fig. S7A). Among the identified motifs, we focused on SOX30, a member of the SOX TF family, as it was highly expressed in spermatocytes and round spermatids and the SOX30 motif was uniquely identified at the one-cell ROSI-high ATAC peaks (Bai et al., 2018; Osaki et al., 1999; Zhang et al., 2018) (Fig. S7B). To examine whether SOX30 was enriched at one-cell ROSI-high ATAC peak regions in round spermatids, we analyzed published SOX30 ChIP-seq data in round spermatids (Chen et al., 2018a). However, the enrichment of SOX30 was weak in these regions (Fig. S7C). Nevertheless, we consider that it would be possible that SOX30 carried over from round spermatids binds to genomic regions where SOX30 did not bind in round spermatids as large-scale chromatin remodelling occurs in early embryos. Next, we attempted to perform immunostaining for SOX30 at the one-cell stage. However, we were not able to detect reliable SOX30 signals in ROSI embryos (Fig. S7D). Although we could not identify factors which contribute to the higher chromatin accessibility in ROSI embryos, it would be important to identify RNAs or proteins transmitted from round spermatids in future studies to comprehensively understand the chromatin alteration in ROSI embryos.

DISCUSSION

To our best knowledge, this is the first report identifying the relationship between altered transcriptome and chromatin accessibility in ROSI embryos. Our transcriptome analysis revealed that ROSI embryos have RNA transmitted from round spermatids, as suggested previously (Hayashi et al., 2003). The number of detected DEGs was limited at the one-cell stage, which is consistent with limited zygotic transcriptional activity during this stage. In contrast, we detected a larger number of DEGs at the two-cell stage, possibly due to a transcriptional burst, called major ZGA, during this stage. Conversely, we found the number of differential accessible regions decreased during transition from one- to two-cell stages (Fig. 3B). Therefore, although defects in chromatin accessibility are corrected to some extent during development, ROSI embryos are likely to suffer from altered gene expression.

Development (2022) 149, dev200696. doi:10.1242/dev.200696

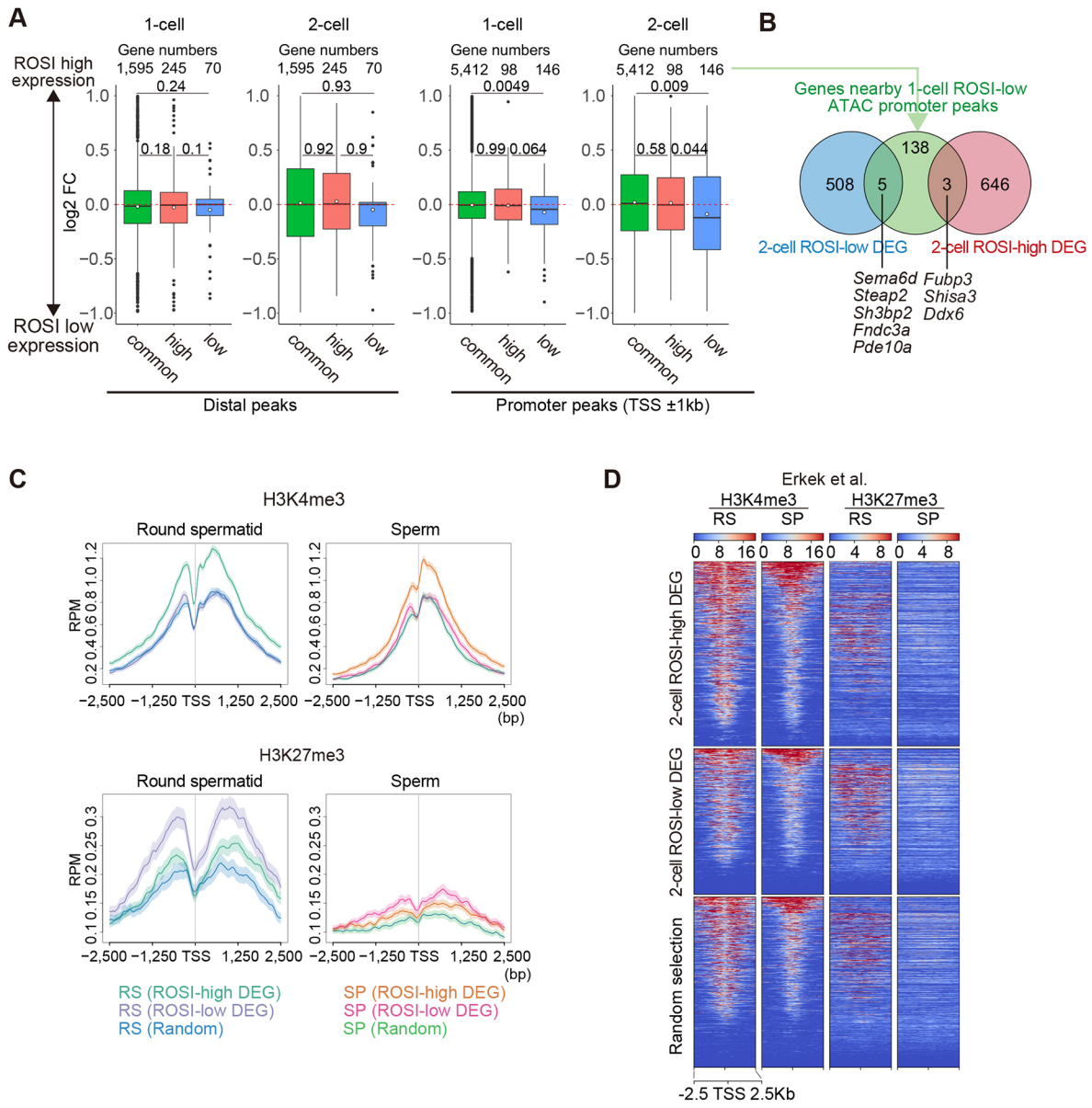

Fig. 5. Altered chromatin accessibility in ROSI embryos affects gene expression. (A) Box plots showing differences in gene expression between ROSI and ICSI embryos at the one- or the two-cell stage. ATAC peak regions were divided into two groups: 'distal' and 'promoter' peaks. Then, the expression was analyzed for the genes associated with the indicated ATAC peak regions defined as 'common', 'high' or 'low' accessibility at distal or promoter peaks. The number of genes in each group is indicated above the box plots. The *P*-values were calculated using Kruskal–Wallis test. Box plots show the distribution of minimum value, first quartile, median, third quartile, maximum value and outliers, and open circles indicate mean value. (B) Venn diagrams showing the overlap between the DEGs in ROSI two-cell embryos and genes associated with one-cell ROSI-low promoter ATAC peaks. The overlapping genes are also indicated. (C,D) Enrichment of H3K4me3 and H3K27me3 in round spermatid (RS) or sperm (SP) around the transcription start sites (TSSs) of the DEGs in two-cell ROSI embryos. Published ChIP-seq data (GSE42629) (Erkek et al., 2013) were used. (C) The enrichment was presented as the average value. H3K4me3 (upper) and H3K27me3 (lower) enrichment in RS (left) and SP (right) around TSS of ROSI-high DEG, ROSI-low DEG and randomly selected genes are coloured differently. ChIP-seq data are shown as RPM. (D) Heatmaps show the enrichment of each DEG group and randomly selected genes as RPKM values.

However, we cannot exclude the possibility that there may be more defects in transcription in one-cell ROSI embryos than detected in this study as it is hard to see a relatively low amount of zygotic transcripts with a conventional RNA-seq at this stage.

By focusing on differentially accessible chromatin regions, we found that lower accessible regions in one-cell ROSI embryos are marked by H3K27me3 in round spermatids. Supporting this observation, we detected the presence of ectopic H3K27me3 in ROSI embryos. This finding prompted us to observe that genes significantly downregulated in ROSI embryos were associated with high levels of H3K27me3 in round spermatids. Therefore, we propose that transmission of H3K27me3 from round spermatids lowers chromatin accessibility at the one-cell stage and alters gene expression profiles at the two-cell stage in ROSI embryos (Fig. 6). This lower accessibility appeared to be corrected at the two-cell stage (Fig. 3C; Fig. S4B). These data suggest that chromatin accessibility at the one-cell stage is important to regulate gene expression at the two-cell stage, although there is still a possibility that ectopic H3K27me3 directly influences gene expression without altering chromatin accessibility at the two-cell stage. We also noticed that lower accessible regions in one-cell ROSI embryos showed high enrichment of H3.3 in sperm, but not in round

Development (2022) 149, dev200696. doi:10.1242/dev.200696

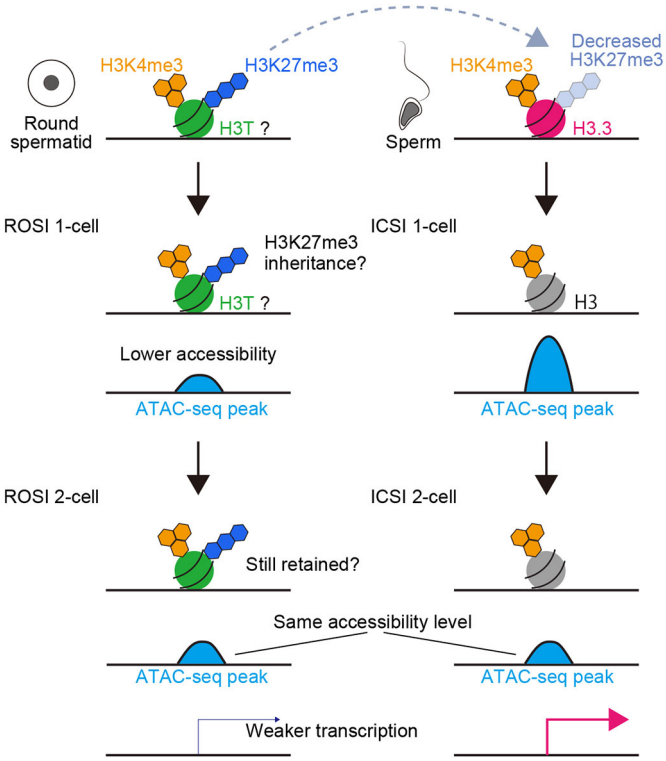

Fig. 6. Model of the effects of epigenetic inheritance from round spermatids on chromatin accessibility and gene expression in ROSI embryos. The promoter regions with lower accessible chromatin regions in ROSI embryos at the one-cell stage correspond to bivalent chromatin regions marked by H3K4me3 and H3K27me3 in round spermatids (left column). The genes associated with this lower accessibility at the one-cell stage were more weakly expressed after cleavage to the two-cell stage, though the differential chromatin accessibility was not observed at the two-cell stage. Note that one-cell embryos have extremely limited transcriptional activity, and thus it is difficult to detect its alteration using a conventional RNA-seq technique employed in this study. Therefore, currently, we cannot exclude the possibility that embryos at the one-cell stage may also have some defect in the expression of these genes. Conversely, these regions are marked by high H3K4me3 and decreased H3K27me3 in sperm, are enriched in H3.3, and show higher accessibility in ICSI one-cell embryos (right column). Therefore, H3K27me3 in round spermatids inherited in ROSI embryos may suppress gene expression. As these regions in sperm are enriched in H3.3, H3K27me3 enrichment may be reduced by replacing H3T with H3.3 during spermiogenesis.

spermatids. During spermiogenesis, histone H3 variant H3T is typically replaced by H3.3, another histone variant (Ueda et al., 2017). Therefore, H3K27me3 is likely to be inherited into ROSI embryos under the absence of this process. Thus, our results highlight the biological significance of chromatin remodelling during spermiogenesis for fine-tuning gene expression after fertilization.

In sperm, H3K27me3 at the one-cell ROSI-low ATAC peak regions decreased, but H3K4me3 was still enriched. Therefore, fertilized embryos inheriting H3.3 marked by H3K4me3 may be advantageous for embryonic gene activation (Fig. 6). These observations imply manipulating H3K27me3 inheritance may help improve low birth rates of ROSI embryos. Recently, a study reported that treating round spermatids with Trichostatin A (TSA) before round spermatids were injected into oocytes improved the development of ROSI embryos to the blastocyst stage (Hosseini and Salehi, 2022). Although exploring whether TSA treatment improves their full-term development is still essential, this method may be useful for identifying potential causes of low birth rates of ROSI embryos. Because previous studies reported that global levels of H3K27me3 decreased following TSA treatment in somatic cell nuclear transfer-derived embryos and ESCs (Karantzali et al., 2008; Selokar et al., 2016), it is possible that improved development of ROSI embryos by TSA is due to reduced H3K27me3 levels in round spermatid. Therefore, identifying the genomic distribution of H3K27me3 in ROSI-derived embryos in an allele-discriminative manner would be crucial given the recent progress in low-input epigenetic analytical techniques. These analyses will clearly pinpoint comprehensive knowledge on not only the causes of low birth rates but also the epigenetic events during spermiogenesis essential for embryonic development.

MATERIALS AND METHODS

Animals and oocyte collection and culture

We used 8- to 12-week-old female ICR (for ATAC-seq; n=247) and C57BL/6 (for RNA-seq; n=72) mice as oocyte donors. Same strain male mice (ICR: n=12, C57BL/6: n=9) were also used as the sperm donor. All animal experiments were approved by the Ethics Committee of the University of Yamanashi (reference number: A29-24) and conducted following Guide for the Care and Use of Laboratory Animals and ARRIVE guidelines. All mice were housed under specific pathogen-free conditions at a constant temperature of 25°C, relative humidity of 50% and a 14 h light/10 h dark period with *ad libitum* access to a commercial diet and distilled water. In this study, body weight was not measured because the body weight of young mice does not affect embryo quality.

ROSI and ICSI

Cumulus cell and oocyte complexes (COCs) were obtained from super-ovulated ICR and C57BL/6 female mice by injection of 7.5 IU equine chorionic gonadotropin (ASKA Pharmaceutical) and human chorionic gonadotropin (ASKA Pharmaceutical) at 46-50 h intervals. Obtained COCs were treated with hyaluronidase for 10 min in HEPES-buffered CZB medium (CZB-HEPES) (Kimura and Yanagimachi, 1995a). For ICSI, sperm were collected from the cauda epididymis, then cultured in human tubal fluid (Quinn et al., 1995) for capacitation for 1 h. Before cytosolic injection of denuded oocytes, sperm tails were eliminated with a Piezo drive micromanipulator (Prime Tech) in CZB-HEPES medium supplemented with 10% PVP (10% PVP-CZB-HEPES). After cutting the tail, the zona pellucida and cytosolic membranes were also disrupted with a Piezo drive micromanipulator. For ROSI, the obtained testes were minced with scissors, sieved through a Mini Cell Strainer and then re-suspended in 10% PVP-CZB-HEPES. The nucleus of each round spermatid was collected with a narrow pipette (7-8 µm diameter). The zona pellucida and cytosolic membrane were disrupted as per the ICSI. The oocytes injected with round spermatid nuclei were activated by culturing in Ca^{2+}-free CZB medium containing 5 mM $SrCl_2$ for 1-2 h.

Removal of PB

Zygotes were treated with cytochalasin B (CB) before elimination for 10-20 min in KSOM, then moved to CB containing CZB-HEPES. The zona pellucida was broken by a Piezo drive micromanipulator. We then vacuumed the second PB with a pipette (10 µm diameter; Fig. 1B). The zona pellucida was solved by Acidic Tyrode. During the wash, the first PB was eliminated by repeated pipetting. Embryos were then cultured in KSOM until sample collection.

Omni-ATAC-seq

We collected 411-450 zygotes and 210-231 two-cell stage ICR embryos (corresponds to 420-462 blastomeres, respectively) for each sample. We then performed omni-ATAC following previously described methods (Corces et al., 2017), with small modifications. To avoid embryo loss, we collected live embryos without PB and zona pellucida, which were transferred into cold ATAC-resuspension buffer and mixed by tapping. After ATAC-reaction for 30 min at 37°C, DNA products were cleaned with a

Development (2022) 149, dev200696. doi:10.1242/dev.200696

MinElute PCR purification kit (Qiagen). We stored 22 µl of the eluted samples at −20°C until subsequent PCR amplification. After five cycles of pre-amplification, we performed an additional PCR for nine cycles. Amplified DNA was purified by a MinElute PCR purification kit. The amplified ATAC-seq libraries were subjected to sequencing by Novaseq 6000 (150-nt paired-end sequencing).

RNA-seq

RNA was extracted from 50 zygotes and 49-96 two-cell stage embryos (C57BL/6 background) with Isogen II (Nippon Gene), according to the manufacturer's instructions. We performed RNA quality analysis on the Bioanalyzer RNA Pico Chip (Agilent Technologies). RNA-seq libraries were constructed by SMART-seq stranded kit with 1 ng of extracted total RNA according to the manufacturer's instructions. RNA fragmentation was then conducted for 2 min. To amplify constructed cDNA, we performed PCR1 (94°C for 1 min, five cycles of 98°C for 15 s, 55°C for 15 s, 68°C for 30 s and 68°C for 2 min) and PCR2 (94°C for 1 min, 14 cycles of 98°C for 15 s, 55°C for 15 s and 68°C for 30 s). The amplified RNA-seq libraries were then subjected to sequencing using Novaseq 6000 (100-nt paired-end sequencing).

Immunostaining

ICSI- and ROSI-derived-zygotes and two-cell stage embryos were collected at 10 and 28-30 hpi or hpa, respectively. Embryos were fixed by 4% paraformaldehyde (PFA) containing 0.2% Triton X-100 (Tx) in PBS, then washed in PBS containing 1% bovine serum albumin (BSA) and 0.2% Tween (Tw) (1% BSA-0.2% Tw). For Sox30 staining, the zona pellucida was removed using Acidic Tyrode after fixation with 4% PFA for 20 min, then the zygotes were permeabilized using PBS containing 0.2% Tx for 20 min. Embryos were then incubated in the following antibodies at 4°C overnight: H3K27me3 rabbit polyclonal antibody (Millipore 07-449, 1:500), H3K9me2 mouse monoclonal antibody (Abcam ab1220, 1:500), Sox30 mouse monoclonal antibody (Santa Cruz Biotechnology sc-390333, 1:500) and H3K9me3 rabbit polyclonal antibody (Abcam ab8898, 1:2000). Embryos were then washed by 1% BSA-0.2% Tw and incubated with secondary antibodies against rabbit or mouse IgG labelled with Alexa Fluor 488, 568 or Cy5 (Invitrogen A11034, A11011, A11001 and Abcam ab97037, 1:500). The immune-stained embryos were then mounted on an antifade mounting medium with DAPI (4′,6-diamidino-2-phenilindole, Vector Laboratories). Fluorescence signals were detected using confocal microscopes FV1000 or FV1200 (Olympus). For quantitative analysis of H3K27me3 levels, we measured fluorescence signal intensity using ImageJ software (Schindelin et al., 2012). We then divided the H3K27me3 signal in each nucleus using the DAPI signal for normalization. Statistical analysis was performed using Prism 9 software (GraphPad). Sperm and round spermatids obtained from minced seminiferous tubules were mounted on slides and fixed in 4% PFA containing 0.2% Tx in PBS for 20 min. Specimens were washed in PBS containing 1% BSA and immunostained for H3K27me3. The H3K27me3 signal in sperm and round spermatids was detected using confocal microscopes FV1200 (Olympus).

Treatment with DRB and quantitative real-time polymerase chain reaction (qRT-PCR)

Ten ICSI or ROSI one-cell embryos at 10 hpi or hpa, respectively, were pooled per sample. To inhibit transcription in ROSI embryos, MII oocytes were cultured in KSOM containing 80 µM DRB (Sigma-Aldrich) before ROSI, and ROSI embryos were then cultured in the presence of DRB.

The samples were added with 5000 copies of H2B-eGFP mRNA (Ooga et al., 2016) as an external control. Quantitative real-time polymerase chain reaction (qRT-PCR) was performed using a CellAmp Direct RNA Prep Kit (TAKARA) and One Step TB Green PrimeScript RT-PCR Kit II (TAKARA) following the manufacturer's instructions. After treatment with DNase I to remove genomic DNA, cell lysates containing total RNA were used as a template for a 10 µl qRT-PCR reaction. The primers used were as follows: *Tp1* (5′-GAGGAGAGGCAAGAACCGAG and 5′-CGGTAATTGCGACTTGCATCA); *Tp2* (5′-GCACTCTCGACACT-CACCTG and 5′-TGTATCTTCGCCCTGAGCTA); *Smcp* (5′-GTTGC-CAGATCAGGAACTCCA and 5′-TGGACAGCACGGTTTAGGTG); eGFP (5′-GCTACCCCGACCACATGAAG and 5′-TCTTGTAGTT-GCCGTCGTCC); *Duxf3* (5′-CCTCAAAGAGGTCCATCAGAGG and 5′-TGAAACCATATGTGGATCGTGTC); MuERV-L (5′-CTCTACCA-CTTGGACCATATGAC and 5′-GAGGCTCCAAACAGCATCTCTA); *Nid2* (5′-CACCGAGGACAGTTTCCATT and 5′-CCAGTTACCAGGT-GCTGGAT); *Klf5* (5′-ACGTACACCATGCCAAGTCA and 5′-GTGGG-AGAGTTGGCGAATTA) (Abe et al., 2018).

ATAC-seq data processing

Adaptor and low-quality sequences were removed by 'fastp' (version 0.20.1) (Chen et al., 2018b) using option '-l 30 -w 10'. Reads were aligned to the mouse genome (mm10) using Bowtie2 (version 2.4.3) (Langmead and Salzberg, 2012) with option '–no-mixed –no-discordant -X 2000' and unmapped reads were discarded by Samtools (version 1.4.1) (Li et al., 2009) with option '-F 0×4'. Reads from PCR duplicates were removed using Picard MarkDuplicates (version 2.23.8) (https://broadinstitute.github.io/picard/). For suiting similar read numbers between replications, reads were divided using 'divide_bam.py' in RseQC (Wang et al., 2012). After confirming reproducibility between replicates, they were merged using Samtools 'merge'. To identify differentially accessible chromatin regions and common peak regions between ROSI and ICSI embryos, each replication peak was first called by MACS2 (version 2.2.7.1) (Zhang et al., 2008) with the option '–nomodel –shift −90 –extsize 180 -f BAMPE -B -q 0.01 -g mm'. Overlapping regions from each replication were then calculated using BEDtools (Quinlan and Hall, 2010) intersect. Overlapping regions and merged read data were used to calculate normalized read density between samples using MAnorm (version 1.3.0) (Shao et al., 2012) and identify differentially accessible chromatin regions under the conditions of FC>1.5 (M-value in MAnorm output data). Published ATAC-seq data (GSE102954, GSE116854, GSE66390) (Jung et al., 2019; Maezawa et al., 2018a; Wu et al., 2016) were also processed similarly and aligned to the mouse genome, as described above. *K*-means clustering and heatmap depiction were conducted using 'computeMatrix' and 'plotHeatmap' in deepTools (version 3.5.1) (Ramírez et al., 2016). ATAC peaks were annotated with nearby genes using annotatePeaks.pl (used GENCODE vM12 database) from HOMER (Heinz et al., 2010) and defined at least ±1.0 kb away from the TSS as distal peaks. 'findMotifsGenome.pl' from HOMER with the default option was used for finding the sequence motif enriched in ATAC-seq peaks.

RNA-seq data processing

Adaptor and low-quality sequences were removed by 'fastp' with the option '-l 50 -w 10'. Reads corresponding to ribosomal RNA were discarded from analysis by extracting reads unmapped to ribosomal DNA using Bowtie2. Subsequently, reads were aligned to the mouse genome (mm10) using STAR (version 2.7.4a) (Dobin et al., 2013). Read counts were calculated using featureCounts (Rsubread version 2.4.3 package in R) (Liao et al., 2014, 2019). To identify DEGs between ROSI and ICSI embryos, the read count data were processed using EdgeR (version 3.32.1) (Robinson et al., 2010). Genes with FDR<0.01 and FC>1.5 or <0.67 were used to identify DEGs. We then performed GO enrichment analyses using DAVID (Huang et al., 2009a,b). Published RNA-seq data (GSE55060, DRA000484 and E-MTAB-2950) (Abe et al., 2015; Hasegawa et al., 2015; Kobayashi et al., 2012) were also processed, as described above. Transcripts per million (TPM) of each gene annotated by GENCODE vM12 was quantified using R (http://www.r-project.org/). The 'cor' and 'hclust' functions with option 'method=ward.D2' in R were used to calculate Spearman rank correlation coefficient and perform hierarchical clustering, respectively. We performed principal component analysis using the 'prcomp' function in R and 'ggplot' (package ggplot2 version 3.3.5) was used for plotting. We performed *k*-means clustering after calculating *z*-scores based on TPM values and heatmaps using the 'pheatmap.type' function (package Pigengene version 1.16.0). Kruskal–Wallis test (Fig. 5A) was performed using the R package 'ggpubr' version 0.4.0.

ChIP-seq data processing

Published ChIP-seq data were obtained from GSE139527, GSE73952, GSE97778, GSE42629, GSE49624, GSE79230, DRA004778 and

GSE107644 (Chen et al., 2018a; Erkek et al., 2013; Hammoud et al., 2014; Ishiuchi et al., 2021; Iwamori et al., 2016; Jung et al., 2017; Liu et al., 2016; Wang et al., 2018). Reads were aligned to the mouse genome (mm10) using Bowtie2 with the option '–no-mixed –no-discordant' after removing adaptor and low-quality sequences using 'fastp'. Unmapped reads were removed using Samtools with option '-F 0×4' and PCR duplicates were removed using Picard MarkDuplicates. Heatmaps were plotted using 'computeMatrix' and 'plotHeatmap' in deepTools. The average read tag density at the promoter region of each DEG group was analyzed using ngs.plot.r (version 2.47.1) (Shen et al., 2014).

Quantification and statistical analysis

Statistical analyses were implemented with R or Prism 9 (GraphPad). Data for two experimental groups were analyzed using a two-tailed Wilcoxon rank-sum test.

Acknowledgements

We thank Drs Satoshi Kamimura, Jafar Sharif, So Maezawa, Akihiko Sakashita, Satoshi Kishigami, Mr Kousuke Kazama, Miss Mayu Tatara and members of the T.W. laboratory and University of Yamanashi, Advanced Biotechnology Centre, for constructive discussions and technical assistance with the NGS analysis.

Competing interests

The authors declare no competing or financial interests.

Author contributions

Conceptualization: T.W., M.O.; Validation: T.K., T.I.; Formal analysis: M.S., T.I.; Investigation: M.S., D.I., R.I., S.W., Y.K., L.Y., E.H., R.E., H.S., T.K., S.H.N., T.I., T.W., M.O.; Resources: D.I., R.I., S.W., Y.K., L.Y., E.H., R.E., H.S., T.W., M.O.; Data curation: M.S., T.I., M.O.; Writing - original draft: M.S., T.I., M.O.; Writing - review & editing: M.S., S.H.N., T.I., M.O.; Visualization: M.S.; Supervision: T.I., T.W., M.O.; Project administration: M.O.; Funding acquisition: T.I., T.W., M.O.

Funding

Financial support for this research was provided by the Japan Society for the Promotion of Science Grant-in-Aid for Young Scientists (19K16012 to M.O.), a Ministry of Education, Culture, Sports, Science and Technology Grant-in-Aid for Scientific Research on Innovative Areas (JP19H05756 to T.I.), the Asada Science Foundation and the Canon Foundation (M20-0006 to T.W.), and the Japan Society for the Promotion of Science KAKENHI [16H06279 (PAGS)].

Data availability

Sequence data reported in this paper are available in The DNA Data Bank of Japan (DDBJ): DRA010218, DRA011368, DRA010219 and DRA011577. Alternatively, all data have also been deposited in Gene Expression Omnibus under accession number GSE196859.

Peer review history

The peer review history is available online at https://journals.biologists.com/dev/lookup/doi/10.1242/dev.200696.reviewer-comments.pdf.

References

Abe, K.-I., Yamamoto, R., Franke, V., Cao, M., Suzuki, Y., Suzuki, M. G., Vlahovicek, K., Svoboda, P., Schultz, R. M. and Aoki, F. (2015). The first murine zygotic transcription is promiscuous and uncoupled from splicing and 3' processing. *EMBO J.* **34**, 1523-1537. doi:10.15252/embj.201490648

Abe, K.-I., Funaya, S., Tsukioka, D., Kawamura, M., Suzuki, Y., Suzuki, M. G., Schultz, R. M. and Aoki, F. (2018). Minor zygotic gene activation is essential for mouse preimplantation development. *Proc. Natl. Acad. Sci. USA* **115**, E6780-E6788. doi:10.1073/pnas.1804309115

Aslam, I., Fishel, S., Green, S., Campbell, A., Garratt, L., McDermott, H., Dowell, K. and Thornton, S. (1998). Can we justify spermatid microinjection for severe male factor infertility? *Hum. Reprod. Update* **4**, 213-222. doi:10.1093/humupd/4.3.213

Bai, S., Fu, K., Yin, H., Cui, Y., Yue, Q., Li, W., Cheng, L., Tan, H., Liu, X., Guo, Y. et al. (2018). Sox30 initiates transcription of haploid genes during late meiosis and spermiogenesis in mouse testes. *Development* **145**, dev164855. doi:10.1242/dev.164855

Burton, A. and Torres-Padilla, M.-E. (2010). Epigenetic reprogramming and development: a unique heterochromatin organization in the preimplantation mouse embryo. *Brief. Funct. Genomics* **9**, 444-454. doi:10.1093/bfgp/elq027

Burton, A., Brochard, V., Galan, C., Ruiz-Morales, E. R., Rovira, Q., Rodriguez-Terrones, D., Kruse, K., Le Gras, S., Udayakumar, V. S., Chin, H. G. et al. (2020). Heterochromatin establishment during early mammalian development is regulated by pericentromeric RNA and characterized by non-repressive H3K9me3. *Nat. Cell Biol.* **22**, 767-778. doi:10.1038/s41556-020-0536-6

Chen, Y., Zheng, Y., Gao, Y., Lin, Z., Yang, S., Wang, T., Wang, Q., Xie, N., Hua, R., Liu, M. et al. (2018a). Single-cell RNA-seq uncovers dynamic processes and critical regulators in mouse spermatogenesis. *Cell Res.* **28**, 879-896. doi:10.1038/s41422-018-0074-y

Chen, S., Zhou, Y., Chen, Y. and Gu, J. (2018b). fastp: an ultra-fast all-in-one FASTQ preprocessor. *Bioinformatics* **34**, i884-i890. doi:10.1093/bioinformatics/bty560

Corces, M. R., Trevino, A. E., Hamilton, E. G., Greenside, P. G., Sinnott-Armstrong, N. A., Vesuna, S., Satpathy, A. T., Rubin, A. J., Montine, K. S., Wu, B. et al. (2017). An improved ATAC-seq protocol reduces background and enables interrogation of frozen tissues. *Nat. Methods* **14**, 959-962. doi:10.1038/nmeth.4396

Dobin, A., Davis, C. A., Schlesinger, F., Drenkow, J., Zaleski, C., Jha, S., Batut, P., Chaisson, M. and Gingeras, T. R. (2013). STAR: ultrafast universal RNA-seq aligner. *Bioinformatics* **29**, 15-21. doi:10.1093/bioinformatics/bts635

Erkek, S., Hisano, M., Liang, C.-Y., Gill, M., Murr, R., Dieker, J., Schübeler, D., van der Vlag, J., Stadler, M. B. and Peters, A. H. F. M. (2013). Molecular determinants of nucleosome retention at CpG-rich sequences in mouse spermatozoa. *Nat. Struct. Mol. Biol.* **20**, 868-875. doi:10.1038/nsmb.2599

Gou, L.-T., Lim, D.-H., Ma, W., Aubol, B. E., Hao, Y., Wang, X., Zhao, J., Liang, Z., Shao, C., Zhang, X. et al. (2020). Initiation of parental genome reprogramming in fertilized oocyte by splicing kinase SRPK1-catalyzed protamine phosphorylation. *Cell* **180**, 1212-1227.e14. doi:10.1016/j.cell.2020.02.020

Hammoud, S. S., Nix, D. A., Zhang, H., Purwar, J., Carrell, D. T. and Cairns, B. R. (2009). Distinctive chromatin in human sperm packages genes for embryo development. *Nature* **460**, 473-478. doi:10.1038/nature08162

Hammoud, S. S., Low, D. H. P., Yi, C., Carrell, D. T., Guccione, E. and Cairns, B. R. (2014). Chromatin and transcription transitions of mammalian adult germline stem cells and spermatogenesis. *Cell Stem Cell* **15**, 239-253. doi:10.1016/j.stem.2014.04.006

Hasegawa, K., Sin, H.-S., Maezawa, S., Broering, T. J., Kartashov, A. V., Alavattam, K. G., Ichijima, Y., Zhang, F., Bacon, W. C., Greis, K. D. et al. (2015). SCML2 establishes the male germline epigenome through regulation of histone H2A ubiquitination. *Dev. Cell* **32**, 574-588. doi:10.1016/j.devcel.2015.01.014

Hayashi, S., Yang, J., Christenson, L., Yanagimachi, R. and Hecht, N. B. (2003). Mouse preimplantation embryos developed from oocytes injected with round spermatids or spermatozoa have similar but distinct patterns of early messenger RNA expression. *Biol. Reprod.* **69**, 1170-1176. doi:10.1095/biolreprod.103.016832

Heinz, S., Benner, C., Spann, N., Bertolino, E., Lin, Y. C., Laslo, P., Cheng, J. X., Murre, C., Singh, H. and Glass, C. K. (2010). Simple combinations of lineage-determining transcription factors prime cis-regulatory elements required for macrophage and B cell identities. *Mol. Cell* **38**, 576-589. doi:10.1016/j.molcel.2010.05.004

Hirabayashi, M., Kato, M., Aoto, T., Ueda, M. and Hochi, S. (2002). Rescue of infertile transgenic rat lines by intracytoplasmic injection of cryopreserved round spermatids. *Mol. Reprod. Dev.* **62**, 295-299. doi:10.1002/mrd.10127

Hosseini, S. and Salehi, M. (2022). Tricostatin A-treated round spermatid enhances preimplantation embryo developmental competency following round spermatid injection in mice. *Zygote* **30**, 373-379. doi:10.1017/S0967199421000836

Huang, D. W., Sherman, B. T. and Lempicki, R. A. (2009a). Systematic and integrative analysis of large gene lists using DAVID bioinformatics resources. *Nat. Protoc.* **4**, 44-57. doi:10.1038/nprot.2008.211

Huang, D. W., Sherman, B. T. and Lempicki, R. A. (2009b). Bioinformatics enrichment tools: paths toward the comprehensive functional analysis of large gene lists. *Nucleic Acids Res.* **37**, 1-13. doi:10.1093/nar/gkn923

Ishiuchi, T., Abe, S., Inoue, K., Yeung, W. K. A., Miki, Y., Ogura, A. and Sasaki, H. (2021). Reprogramming of the histone H3.3 landscape in the early mouse embryo. *Nat. Struct. Mol. Biol.* **28**, 38-49. doi:10.1038/s41594-020-00521-1

Iwamori, N., Tominaga, K., Sato, T., Riehle, K., Iwamori, T., Ohkawa, Y., Coarfa, C., Ono, E. and Matzuk, M. M. (2016). MRG15 is required for pre-mRNA splicing and spermatogenesis. *Proc. Natl. Acad. Sci. USA* **113**, E5408-E5415. doi:10.1073/pnas.1611995113

Jung, Y. H., Sauria, M. E. G., Lyu, X., Cheema, M. S., Ausio, J., Taylor, J. and Corces, V. G. (2017). Chromatin states in mouse sperm correlate with embryonic and adult regulatory landscapes. *Cell Rep.* **18**, 1366-1382. doi:10.1016/j.celrep.2017.01.034

Jung, Y. H., Kremsky, I., Gold, H. B., Rowley, M. J., Punyawai, K., Buonanotte, A., Lyu, X., Bixler, B. J., Chan, A. W. S. and Corces, V. G. (2019). Maintenance of CTCF- and transcription factor-mediated interactions from the gametes to the early mouse embryo. *Mol. Cell* **75**, 154-171.e5. doi:10.1016/j.molcel.2019.04.014

Karantzali, E., Schulz, H., Hummel, O., Hubner, N., Hatzopoulos, A. and Kretsovali, A. (2008). Histone deacetylase inhibition accelerates the early events

of stem cell differentiation: transcriptomic and epigenetic analysis. *Genome Biol.* **9**, R65. doi:10.1186/gb-2008-9-4-r65

Kimura, Y. and Yanagimachi, R. (1995a). Intracytoplasmic sperm injection in the mouse. *Biol. Reprod.* **52**, 709-720. doi:10.1095/biolreprod52.4.709

Kimura, Y. and Yanagimachi, R. (1995b). Mouse oocytes injected with testicular spermatozoa or round spermatids can develop into normal offspring. *Development* **121**, 2397-2405. doi:10.1242/dev.121.8.2397

Kishigami, S., Van Thuan, N., Hikichi, T., Ohta, H., Wakayama, S., Mizutani, E. and Wakayama, T. (2006). Epigenetic abnormalities of the mouse paternal zygotic genome associated with microinsemination of round spermatids. *Dev. Biol.* **289**, 195-205. doi:10.1016/j.ydbio.2005.10.026

Kobayashi, H., Sakurai, T., Imai, M., Takahashi, N., Fukuda, A., Yayoi, O., Sato, S., Nakabayashi, K., Hata, K., Sotomaru, Y. et al. (2012). Contribution of intragenic DNA methylation in mouse gametic DNA methylomes to establish oocyte-specific heritable marks. *PLoS Genet.* **8**, e1002440. doi:10.1371/journal.pgen.1002440

Langmead, B. and Salzberg, S. L. (2012). Fast gapped-read alignment with Bowtie 2. *Nat. Methods* **9**, 357-359. doi:10.1038/nmeth.1923

Lesch, B. J., Dokshin, G. A., Young, R. A., McCarrey, J. R. and Page, D. C. (2013). A set of genes critical to development is epigenetically poised in mouse germ cells from fetal stages through completion of meiosis. *Proc. Natl. Acad. Sci. USA* **110**, 16061-16066. doi:10.1073/pnas.1315204110

Lesch, B. J., Silber, S. J., McCarrey, J. R. and Page, D. C. (2016). Parallel evolution of male germline epigenetic poising and somatic development in animals. *Nat. Genet.* **48**, 888-894. doi:10.1038/ng.3591

Li, H., Handsaker, B., Wysoker, A., Fennell, T., Ruan, J., Homer, N., Marth, G., Abecasis, G. and Durbin, R. and **1000 Genome Project Data Processing Subgroup.** (2009). The sequence alignment/map format and SAMtools. *Bioinformatics* **25**, 2078-2079. doi:10.1093/bioinformatics/btp352

Liao, Y., Smyth, G. K. and Shi, W. (2014). featureCounts: an efficient general purpose program for assigning sequence reads to genomic features. *Bioinformatics* **30**, 923-930. doi:10.1093/bioinformatics/btt656

Liao, Y., Smyth, G. K. and Shi, W. (2019). The R package Rsubread is easier, faster, cheaper and better for alignment and quantification of RNA sequencing reads. *Nucleic Acids Res.* **47**, e47. doi:10.1093/nar/gkz114

Lismer, A., Siklenka, K., Lafleur, C., Dumeaux, V. and Kimmins, S. (2020). Sperm histone H3 lysine 4 trimethylation is altered in a genetic mouse model of transgenerational epigenetic inheritance. *Nucleic Acids Res.* **48**, 11380-11393. doi:10.1093/nar/gkaa712

Liu, X., Wang, C., Liu, W., Li, J., Li, C., Kou, X., Chen, J., Zhao, Y., Gao, H., Wang, H. et al. (2016). Distinct features of H3K4me3 and H3K27me3 chromatin domains in pre-implantation embryos. *Nature* **537**, 558-562. doi:10.1038/nature19362

Maezawa, S., Yukawa, M., Alavattam, K. G., Barski, A. and Namekawa, S. H. (2018a). Dynamic reorganization of open chromatin underlies diverse transcriptomes during spermatogenesis. *Nucleic Acids Res.* **46**, 593-608. doi:10.1093/nar/gkx1052

Maezawa, S., Hasegawa, K., Yukawa, M., Kubo, N., Sakashita, A., Alavattam, K. G., Sin, H.-S., Kartashov, A. V., Sasaki, H., Barski, A. et al. (2018b). Polycomb protein SCML2 facilitates H3K27me3 to establish bivalent domains in the male germline. *Proc. Natl. Acad. Sci. USA* **115**, 4957-4962. doi:10.1073/pnas.1804512115

Ogura, A., Matsuda, J. and Yanagimachi, R. (1994). Birth of normal young after electrofusion of mouse oocytes with round spermatids. *Proc. Natl. Acad. Sci. USA* **91**, 7460-7462. doi:10.1073/pnas.91.16.7460

Ooga, M., Fulka, H., Hashimoto, S., Suzuki, M. G. and Aoki, F. (2016). Analysis of chromatin structure in mouse preimplantation embryos by fluorescent recovery after photobleaching. *Epigenetics* **11**, 85-94. doi:10.1080/15592294.2015.1136774

Osaki, E., Nishina, Y., Inazawa, J., Copeland, N. G., Gilbert, D. J., Jenkins, N. A., Ohsugi, M., Tezuka, T., Yoshida, M. and Semba, K. (1999). Identification of a novel Sry-related gene and its germ cell-specific expression. *Nucleic Acids Res.* **27**, 2503-2510. doi:10.1093/nar/27.12.2503

Quinlan, A. R. and Hall, I. M. (2010). BEDTools: a flexible suite of utilities for comparing genomic features. *Bioinformatics* **26**, 841-842. doi:10.1093/bioinformatics/btq033

Quinn, P., Moinipanah, R., Steinberg, J. M. and Weathersbee, P. S. (1995). Successful human in vitro fertilization using a modified human tubal fluid medium lacking glucose and phosphate ions. *Fertil. Steril.* **63**, 922-924. doi:10.1016/S0015-0282(16)57504-9

Ramírez, F., Ryan, D. P., Grüning, B., Bhardwaj, V., Kilpert, F., Richter, A. S., Heyne, S., Dündar, F. and Manke, T. (2016). deepTools2: a next generation web server for deep-sequencing data analysis. *Nucleic Acids Res.* **44**, W160-W165. doi:10.1093/nar/gkw257

Rathke, C., Baarends, W. M., Awe, S. and Renkawitz-Pohl, R. (2014). Chromatin dynamics during spermiogenesis. *Biochim. Biophys. Acta Gene Regul. Mech.* **1839**, 155-168. doi:10.1016/j.bbagrm.2013.08.004

Robinson, M. D., McCarthy, D. J. and Smyth, G. K. (2010). edgeR: a bioconductor package for differential expression analysis of digital gene expression data. *Bioinformatics* **26**, 139-140. doi:10.1093/bioinformatics/btp616

Schindelin, J., Arganda-Carreras, I., Frise, E., Kaynig, V., Longair, M., Pietzsch, T., Preibisch, S., Rueden, C., Saalfeld, S., Schmid, B. et al. (2012). Fiji: an open-source platform for biological-image analysis. *Nat. Methods* **9**, 676-682. doi:10.1038/nmeth.2019

Selokar, N. L., Saini, M., Agrawal, H., Palta, P., Chauhan, M. S., Manik, R. and Singla, S. K. (2016). Buffalo (Bubalus bubalis) SCNT embryos produced from somatic cells isolated from frozen-thawed semen: effect of trichostatin A on the in vitro and in vivo developmental potential, quality and epigenetic status. *Zygote* **24**, 549-553. doi:10.1017/S0967199415000520

Shao, Z., Zhang, Y., Yuan, G.-C., Orkin, S. H. and Waxman, D. J. (2012). MAnorm: a robust model for quantitative comparison of ChIP-Seq data sets. *Genome Biol.* **13**, R16. doi:10.1186/gb-2012-13-3-r16

Shen, L., Shao, N., Liu, X. and Nestler, E. (2014). ngs.plot: quick mining and visualization of next-generation sequencing data by integrating genomic databases. *BMC Genomics* **15**, 284. doi:10.1186/1471-2164-15-284

Siklenka, K., Erkek, S., Godmann, M., Lambrot, R., McGraw, S., Lafleur, C., Cohen, T., Xia, J., Suderman, M., Hallett, M. et al. (2015). Disruption of histone methylation in developing sperm impairs offspring health transgenerationally. *Science* **350**, aab2006. doi:10.1126/science.aab2006

Sin, H.-S., Kartashov, A. V., Hasegawa, K., Barski, A. and Namekawa, S. H. (2015). Poised chromatin and bivalent domains facilitate the mitosis-to-meiosis transition in the male germline. *BMC Biol.* **13**, 53. doi:10.1186/s12915-015-0159-8

Sofikitis, N. V., Miyagawa, I., Agapitos, E., Pasyianos, P., Toda, T., Hellstrom, W. J. and Kawamura, H. (1994). Reproductive capacity of the nucleus of the male gamete after completion of meiosis. *J. Assist. Reprod. Genet.* **11**, 335-341. doi:10.1007/BF02214138

Tanaka, A., Nagayoshi, M., Takemoto, Y., Tanaka, I., Kusunoki, H., Watanabe, S., Kuroda, K., Takeda, S., Ito, M. and Yanagimachi, R. (2015). Fourteen babies born after round spermatid injection into human oocytes. *Proc. Natl. Acad. Sci. USA* **112**, 14629-14634. doi:10.1073/pnas.1517466112

Tanaka, A., Suzuki, K., Nagayoshi, M., Tanaka, A., Takemoto, Y., Watanabe, S., Takeda, S., Irahara, M., Kuji, N., Yamagata, Z. et al. (2018). Ninety babies born after round spermatid injection into oocytes: survey of their development from fertilization to 2 years of age. *Fertil. Steril.* **110**, 443-451. doi:10.1016/j.fertnstert.2018.04.033

Tatehana, M., Kimura, R., Mochizuki, K., Inada, H. and Osumi, N. (2020). Comprehensive histochemical profiles of histone modification in male germline cells during meiosis and spermiogenesis: comparison of young and aged testes in mice. *PLoS One* **15**, e0230930. doi:10.1371/journal.pone.0230930

Tekayev, M. and Vuruskan, A. K. (2021). Clinical values and advances in round spermatid injection (ROSI). *Reprod. Biol.* **21**, 100530. doi:10.1016/j.repbio.2021.100530

Teperek, M., Simeone, A., Gaggioli, V., Miyamoto, K., Allen, G. E., Erkek, S., Kwon, T., Marcotte, E. M., Zegerman, P., Bradshaw, C. R. et al. (2016). Sperm is epigenetically programmed to regulate gene transcription in embryos. *Genome Res.* **26**, 1034-1046. doi:10.1101/gr.201541.115

Tesarik, J., Mendoza, C. and Testart, J. (1995). Viable embryos from injection of round spermatids into oocytes. *N. Engl. J. Med.* **333**, 525. doi:10.1056/NEJM199508243330819

Tesarik, J., Rolet, F., Brami, C., Sedbon, E., Thorel, J., Tibi, C. and Thébault, A. (1996). Spermatid injection into human oocytes. II. Clinical application in the treatment of infertility due to non-obstructive azoospermia. *Hum. Reprod.* **11**, 780-783. doi:10.1093/oxfordjournals.humrep.a019254

Ueda, J., Harada, A., Urahama, T., Machida, S., Maehara, K., Hada, M., Makino, Y., Nogami, J., Horikoshi, N., Osakabe, A. et al. (2017). Testis-specific histone variant H3t gene is essential for entry into spermatogenesis. *Cell Rep.* **18**, 593-600. doi:10.1016/j.celrep.2016.12.065

Wang, L., Wang, S. and Li, W. (2012). RSeQC: quality control of RNA-seq experiments. *Bioinformatics* **28**, 2184-2185. doi:10.1093/bioinformatics/bts356

Wang, C., Liu, X., Gao, Y., Yang, L., Li, C., Liu, W., Chen, C., Kou, X., Zhao, Y., Chen, J. et al. (2018). Reprogramming of H3K9me3-dependent heterochromatin during mammalian embryo development. *Nat. Cell Biol.* **20**, 620-631. doi:10.1038/s41556-018-0093-4

Wu, J., Huang, B., Chen, H., Yin, Q., Liu, Y., Xiang, Y., Zhang, B., Liu, B., Wang, Q., Xia, W. et al. (2016). The landscape of accessible chromatin in mammalian preimplantation embryos. *Nature* **534**, 652-657. doi:10.1038/nature18606

Yamaguchi, K., Hada, M., Fukuda, Y., Inoue, E., Makino, Y., Katou, Y., Shirahige, K. and Okada, Y. (2018). Re-evaluating the localization of sperm-retained histones revealed the modification-dependent accumulation in specific genome regions. *Cell Rep.* **23**, 3920-3932. doi:10.1016/j.celrep.2018.05.094

Yoshida, K., Muratani, M., Araki, H., Miura, F., Suzuki, T., Dohmae, N., Katou, Y., Shirahige, K., Ito, T. and Ishii, S. (2018). Mapping of histone-binding sites in histone replacement-completed spermatozoa. *Nat. Commun.* **9**, 3885. doi:10.1038/s41467-018-06243-9

Zhang, Y., Liu, T., Meyer, C. A., Eeckhoute, J., Johnson, D. S., Bernstein, B. E., Nusbaum, C., Myers, R. M., Brown, M., Li, W. et al. (2008). Model-based analysis of ChIP-Seq (MACS). *Genome Biol.* **9**, R137. doi:10.1186/gb-2008-9-9-r137

Zhang, T., Cooper, S. and Brockdorff, N. (2015). The interplay of histone modifications – writers that read. *EMBO Rep.* **16**, 1467-1481. doi:10.15252/embr.201540945

Zhang, B., Zheng, H., Huang, B., Li, W., Xiang, Y., Peng, X., Ming, J., Wu, X., Zhang, Y., Xu, Q. et al. (2016). Allelic reprogramming of the histone modification H3K4me3 in early mammalian development. *Nature* **537**, 553-557. doi:10.1038/nature19361

Zhang, D., Xie, D., Lin, X., Ma, L., Chen, J., Zhang, D., Wang, Y., Duo, S., Feng, Y., Zheng, C. et al. (2018). The transcription factor SOX30 is a key regulator of mouse spermiogenesis. *Development* **145**, dev164723. doi:10.1242/dev.164723

Zhao, M., Shirley, C. R., Mounsey, S. and Meistrich, M. L. (2004). Nucleoprotein transitions during spermiogenesis in mice with transition nuclear protein Tnp1 and Tnp2 mutations. *Biol. Reprod.* **71**, 1016-1025. doi:10.1095/biolreprod.104.028191